nature biomedical engineering

PERSPECTIVE

https://doi.org/10.1038/s41551-021-00808-8

Check for updates

Intraoperative imaging in pathology-assisted surgery

Floris J. Voskuil[1,2,11], Jasper Vonk[1,11], Bert van der Vegt[2], Schelto Kruijff[3,4], Vasilis Ntziachristos[5,6], Pieter J. van der Zaag[7,9,10], Max J. H. Witjes[1] and Gooitzen M. van Dam[4,8] ✉

The pathological assessment of surgical specimens during surgery can reduce the incidence of positive resection margins, which otherwise can result in additional surgeries or aggressive therapeutic regimens. To improve patient outcomes, intraoperative spectroscopic, fluorescence-based, structural, optoacoustic and radiological imaging techniques are being tested on freshly excised tissue. The specific clinical setting and tumour type largely determine whether endogenous or exogenous contrast is to be detected and whether the tumour specificity of the detected biomarker, image resolution, image-acquisition times or penetration depth are to be prioritized. In this Perspective, we describe current clinical standards for intraoperative tissue analysis and discuss how intraoperative imaging is being implemented. We also discuss potential implementations of intraoperative pathology-assisted surgery for clinical decision-making.

In surgical oncology, the ideal surgical outcome is the resection of the entire tumour bulk and the preservation of the adjacent (healthy) tissue. However, the occurrence of tumour-positive surgical margins—where histological analysis shows the presence of tumour cells close to the edge of the resected tissue (Box 1)—ranges from approximately 10% to 35% of surgeries, depending on the tumour type[1]. This can increase the rates of local recurrence and distant metastases, and decrease survival[2–8]. Although complete tumour resection is crucial, tumour delineation during the surgical procedure and post-operative pathological assessment generally involves decades-old techniques, as well as visual and tactile information obtained by the practitioner[9].

The current standard of care for intraoperative surgical guidance is the fresh frozen sectioning (FFS) of tissue biopsies (Box 2). Although helpful in some cases, this technique usually requires up to 1 h and is only available for the analysis of small tissue biopsies. Unfortunately, the reliability of FFS for margin assessment is controversial, as it is susceptible to sampling error. Also, the technical quality of FFS is low compared to definitive histopathology. Indeed, discrepancies of up to 12.9% cases between FFS and final histopathology on margin status is possible[10–14]. Moreover, margin assessments of the entire excision specimen can take up several days (Table 1), which precludes the possibility of altering the initial treatment plan or of intervening immediately during the initial surgery. When the final histopathology results are available, a second treatment (if possible at all because of typically altered anatomy and distortion of the initial anatomical orientation, as occurs with the collapse of the surgical cavity in breast-cancer surgery and brain surgery) often leads to overtreatment. This can involve mutilating surgical procedures or chemoradiotherapy to correct for an incomplete initial surgery[2–6,8].

Computed tomography (CT), magnetic resonance imaging (MRI) and ultrasound support surgery by providing pre-operative information. Yet reliable imaging techniques that generate real-time information for clinical decision-making during surgery have not been widely adopted. They could, however, provide two major advantages for the patient: the ability to detect loco-regional metastases, which would greatly influence the treatment strategy during surgery; and the early detection of tumour-positive margins, which would enable the immediate resection of additional tumour tissue during the first surgery.

The need for real-time information has led to increasing interest in intraoperative in vivo imaging techniques that can guide surgeons during a surgical procedure by providing information that the human eye cannot detect[15–20]. For example, in surgical oncology, in vivo imaging can detect unknown or additional tumour lesions or guide the surgeon to determine the resection margin to avoid the unnecessary removal of normal tissue. However, the use of in vivo imaging techniques is constrained by regulatory concerns inherent to a sterile working environment. Also, variations in image-acquisition settings related to the surgical working area, and the absence of standardization and calibration protocols for existing imaging systems, have resulted in a lack of benchmarking and of quality controls. All these factors can have serious impacts on margin assessment, in particular because signal inhomogeneities can lead to erroneous tumour delineation[21–23]. These limitations can be redressed through the pathological assessment of excised tissue immediately after resection while the patient is still anaesthetized. Indeed, the assessment of the excised specimen outside the sterile surgical working area enables more rigorous standardization of the imaging procedures. That is, the process is less susceptible to regulatory issues and still provides immediate feedback to the attending

[1]Department of Oral and Maxillofacial Surgery, University of Groningen, University Medical Center Groningen, Groningen, The Netherlands. [2]Department of Pathology and Medical Biology, University of Groningen, University Medical Center Groningen, Groningen, The Netherlands. [3]Department of Surgery, University of Groningen, University Medical Center Groningen, Groningen, The Netherlands. [4]Department of Nuclear Medicine and Molecular Imaging, University of Groningen, University Medical Center Groningen, Groningen, The Netherlands. [5]Chair for Biological Imaging, Center for Translational Cancer Research, Technical University of Munich, Klinikum rechts der Isar, Munich, Germany. [6]Institute of Biological and Medical Imaging, Helmholtz Zentrum München, Neuherberg, Germany. [7]Phillips Research Laboratories, Eindhoven, The Netherlands. [8]AxelaRx/TRACER BV, Groningen, The Netherlands. [9]Present address: Department of Nuclear Medicine and Molecular Imaging, University of Groningen, University Medical Center Groningen, Groningen, The Netherlands. [10]Present address: Molecular Biophysics, Zernike Institute, University of Groningen, Groningen, The Netherlands. [11]These authors contributed equally: Floris J. Voskuil, Jasper Vonk. ✉e-mail: g.m.van.dam@umcg.nl

Box 1 | Adequate resection margins in surgical oncology

A tumour-positive margin is defined by the presence of tumour cells in the surgical margin. However, a tumour-negative margin does not imply the absence of tumour cells in the margin. In fact, the exact definition of a tumour-negative surgical margin is specific to the tumour type (Table 1). In general, two protocols are used: no tumour cells present at the edge of the excised specimen (no ink on tumour) or no tumour cells within 1 mm of the cut surface[166,173–176]. For some tumour types, however, an adequate margin is defined as ≥5 mm because close margins of <5 mm can cause metastasis (loco-regional or otherwise) for some tumour types[1] and are therefore an indication for the need for adjuvant therapies (such as radiation or chemoradiation)[13]. Consequently, the optimal imaging technique for margin assessment also depends on the tumour type and on the required imaging depth.

Box 2 | Standards for the tissue processing of excised surgical specimens

The general principles associated with the evaluation of excised specimens substantially overlap between countries and hospitals. Supporting surgery with pathology is a dynamic process that begins with the first incision. Surgical guidance is often necessary during surgical margin assessment or when the surgical strategy (that is, 'where to cut?') is determined using FFS analysis. Although FFS usually provides feedback to the surgeon within 1 h, it is prone to sampling error, as only a fraction of the excised tissue is examined and tumour can be missed, which can lead to misinterpretation of the true margin status. A discordance between FFS and definitive histopathology occurs in approximately 5% of the cases, but can be as high as 12.9%[10–14].

After excision, the surgeon immediately assesses the margins by visual and tactile inspection of the surgical specimen to determine whether immediate re-resection is necessary. To communicate with the pathologist, the surgeon can use tags (such as pins or stiches) to designate important structures or locations on the specimen for anatomical orientation purposes (for example, a stitch at the craniomedial side on a lumpectomy specimen or on an area where there is uncertainty about tumour-free margins). Subsequently, the specimen is submitted to the pathology department either immediately after resection or at the end of the surgical procedure. At the pathology department, white-light images are taken for anatomical orientation purposes and for the pathological-assessment phases, which are typically carried out at a later point. In most cases, the specimen is formalin-fixed for 24–48 h, depending on the tissue type and the tissue size. After fixation (sometimes earlier), the specimen is manually cut into tissue slices of approximately 5–10 mm. The pathologist manually and visually selects which tissue slices have to be analysed microscopically. These selected slices are then processed into formalin-fixed paraffin-embedded blocks (usually overnight), and then one or more 3–5-μm thin sections are cut for haematoxylin and eosin (H&E) staining or for staining with specific immunohistochemistry agents. The H&E sections are examined microscopically (conventionally or digitally) by the pathologist. The final histopathological report may not be available until up to five working days after the surgery. The procedure is prone to sampling errors.

surgeons, which then allows for additional intraoperative intervention if needed. However, little research to this effect has been carried out to date. Although several studies have reported technical innovations in imaging techniques[24–28], few clinical trials assessing the impact of intraoperative imaging techniques on surgical outcomes have been carried out[29].

Table 1 | International definitions for tumour-positive resection margins

Tumour	Positive margin	International consensus
Breast	Ink on tumour[5]	Internationally accepted.
Colorectal	<1 mm for proximal and circumferential resection margins	Internationally accepted.
Oesophageal	Ink on tumour[164,165] for proximal and distal margins <1 mm (ref. [164]) or ink on tumour[165] for circumferential resection margins	The definitions used by the Royal College of Pathologists and College of American Pathologists vary.
Head-and-neck squamous cell carcinoma	<1 mm (close margin, <5 mm)[13]	Internationally accepted.
Prostate	Ink on tumour[166]	Internationally accepted.
Ovarian	Not reported	Resection margins are not reported because the surgical approach is focused on cytoreduction.
Vulva	<8 mm (ref. [167])[a]	Internationally accepted.
Melanoma	<5 mm (ref. [168])	Internationally accepted.
Sarcoma	Ink on tumour[169]	Internationally accepted.
Glioblastoma	Ink on tumour (the tumour is usually not excised as one intact specimen)[170]	Internationally accepted.
Lung	Ink on tumour[171]	Internationally accepted.
Pancreatic	<1 mm (ref. [172])	Internationally accepted, although there is controversy over the definition of an adequate margin. Officially, a tumour-positive margin is defined as ink on tumour. However, growing evidence indicates that <1 mm should be used as a cut-off point to distinguish between adequate and non-adequate resections.

[a]As determined on formalin-fixed tissue, which corresponds to a 1-cm surgical margin.

In this Perspective, we discuss the current status of intraoperative tissue analysis in the surgical theatre, and provide an overview of the imaging techniques—spectroscopic, fluorescence-based, structural, optoacoustic and radiological—that could assist clinical decision-making based on the ex vivo evaluation of excised tissue. Moreover, by describing three typical scenarios of use, we discuss how the intraoperative implementation of techniques of intraoperative pathology-assisted surgery (IPAS)—that is, the real-time collaboration between surgeons and pathologists—could affect surgical treatment strategies.

Current status of IPAS

Intraoperative clinical decision-making is never based on a single parameter, especially for a patient with cancer who may be suffering from comorbidities at the time of surgery. For instance, the current health status of the patient and any unexpected findings can play a role. In fact, intraoperative findings after excision of the tissue can

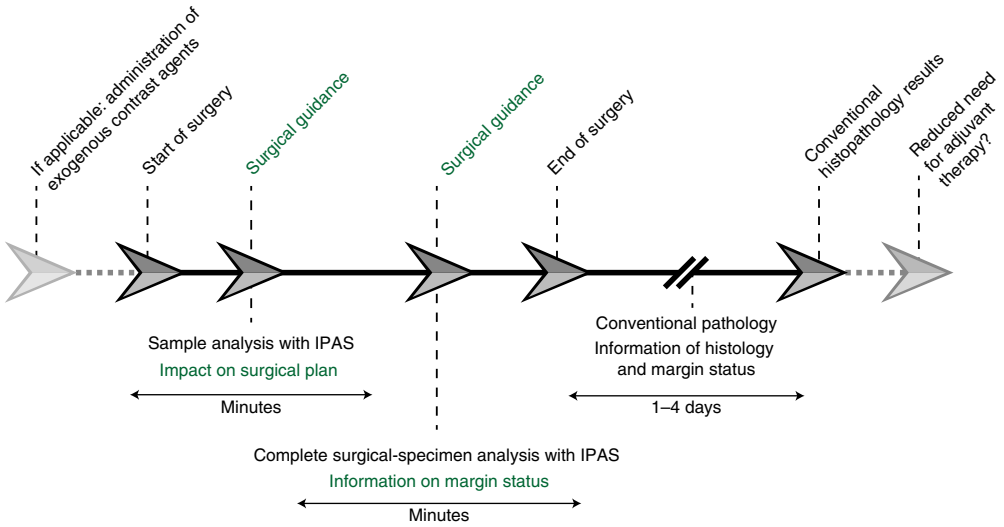

Fig. 1 | Flowchart for IPAS. The implementation of IPAS (green text) may enhance surgical guidance for surgical planning and margin assessment in excised surgical specimens. By providing feedback within minutes, intraoperative imaging could reduce the need for adjuvant therapy or re-excision surgeries to correct for incomplete tumour resection.

severely affect the treatment strategy. Two types of IPAS are generally used to guide the attending surgeon in clinical decision-making: the evaluation of a small tissue biopsy for the presence of tumour cells, or the use of a whole specimen for margin assessment (Fig. 1).

Evaluation of small tissue biopsies. At present, the only clinically approved method for intraoperative pathology-assisted guidance is an intraoperatively collected small tissue biopsy analysed using FSS[10–14]. There are three indications for performing an intraoperative biopsy: the absence of histological information available about an intraoperatively detected lesion; insufficient information available on the geometry of the primary tumour lesion; and whether the assessment of lymph nodes (to assess any metastatic involvement) is required. For example, tissue biopsies can be performed to evaluate the planned resection margin; however, this approach cannot assess the depth of the resection. Moreover, random or targeted biopsies can be performed to assess the presence of locoregional or distant metastasis. Clinical indications for obtaining small tissue biopsies may vary, yet the requirements for a set of tools to assess small tissue biopsies are identical: the image resolution has to be sufficiently high to enable the detection of small tumour lesions that may affect the treatment strategy[30]. High image-resolution requirements usually result in lower imaging rates; still, samples smaller than 1 cm^2 can be imaged within minutes.

Margin assessment in whole specimens. The analysis of a whole specimen differs from that of a small biopsy in several ways. In most cases, the attending surgeon is aware of the underlying pathology of the excised specimen. However, determining the extent of the disease remains challenging, even with extensive pre-operative imaging[31]. Real-time feedback of the status of the resection margins demands a technique that analyses the entire resection surface within a time frame that allows for the surgeon to act. Ideally, an IPAS technique for rapid ex vivo tissue analysis would provide an image of a large surface (of the order of tens of square centimetres) within minutes. However, because the definition of a tumour-positive margin varies between tumour types (Table 1), different penetration depths may be clinically required. Imaging speed can be enhanced at lower imaging resolutions, and low-resolution imaging may sometimes be sufficient for identifying the potential areas at risk within minutes (this strategy is known as red-flag detection[32]). If necessary, subsequent analysis at a higher resolution can be carried out to assess the detected lesion microscopically. In fact, multimodal imaging could often be advantageous for margin evaluation in whole specimens.

Imaging techniques

A diverse set of tissue characteristics and components can be optically detected to assist intraoperative pathology. In general, there are two imaging strategies: the visualization of endogenous tissue characteristics, and the visualization of exogenous contrast agents to highlight otherwise invisible tissue characteristics. On the one hand, an advantage of visualizing endogenous tissue characteristics[33–36] is that the imaging process does not require a contrast agent and does not interfere with the environment or microenvironment of interest. However, only a limited range of biological characteristics (usually related to metabolism[34] and oxygenation[35]) and tissues[33,37,38] can be visualized by means of endogenous contrast. On the other hand, targeted exogenous contrast agents can increase the tumour specificity of the signal. Exogenous contrast agents consist of a signalling compound (a fluorophore or absorber)[22,39–41] and a targeting moiety (small peptides, monoclonal antibodies[15,42], nanobodies[43], nanoparticles[44] or activatable optical tracers[45]).

Spectroscopy imaging. Generally, spectroscopy imaging refers to the detection of superficial signals 'reflected' from tissue. Spectroscopy methods obtain measurements from tissue at multiple spectral regions and analyse the collected spectra to identify cellular density or biochemical information. High spectral resolution is possible by collecting spectra covering a wavelength range of hundreds of nanometres; however, higher spectral resolution results in lower imaging speed. Various spectroscopy approaches[46] can be used as two-dimensional scans to generate spectroscopy images.

Hyperspectral imaging (HSI), which was initially developed by NASA (the National Aeronautics and Space Administration)[47], has been considered for various clinical applications[48]. HSI can provide diagnostic information on tissue composition for pathologies with a different optical fingerprint to healthy tissue[49]. The images are reconstructed by combining two spatial dimensions and a third spectral dimension (referred to as a hyperspectral cube). HSI can be used to spatially delineate tumours without the need for exogenous contrast[48]. HSI has been used on fresh tissue samples from various

tumour types (in particular, head-and-neck cancer[50–54], thyroid cancer[51,53] and colorectal cancer[55]) with accuracies of 81–94%[50–55]. HSI has also been used intraoperatively in patients with tongue cancer by using light that covered the visible and near-infrared (NIR) spectra. Specifically, immediately after resection, a freshly excised surgical specimen was bisected along the middle of the tumour, and the cut surface was imaged with both visible-light HSI (450–1,000 nm) and NIR HSI (950–1,700 nm). Subsequently, a trained neural network discriminated between tumour tissue and healthy muscle tissue with a combined accuracy (for visible-light and NIR data) of 82.3%[56]. An imaging depth of 2 mm was obtained with the visible-light HSI camera system[57], which enabled adequate margin assessment for some tumour types (Table 1). Specimen margins during lumpectomy have also been assessed by HSI[58]. Images of the complete fresh surgical margin were obtained within 10 min. A classification algorithm detected all but one tumour-positive margins in 20 lumpectomy specimens. Specifically, except for one tumour (which was smaller than 1 mm^2), the results from HSI and conventional H&E histology correlated for tumours within 2 mm of the resection surface.

Raman imaging can provide information on the chemical composition of tissue by analysing molecule vibrations (referred to as Raman scattering)[59]. Raman techniques offer label-free molecular contrast, albeit with low signal-to-noise ratio, owing to weak Raman scattering cross-sections. Conventional Raman imaging based on spontaneous Raman scattering has been used to detect oral cancer[60–62] and soft tissue sarcoma[63], but showed limited accuracy and required long acquisition times (0.2–30 s per measurement[64]), which may have hampered their clinical implementation[65]. Coherent Raman-based techniques, including coherent anti-Stokes Raman scattering (CARS) and stimulated Raman scattering (SRS) microscopy, provide a larger (orders of magnitude) increase in image-acquisition speed owing to coherent signal generation[66,67]. Consequently, these techniques can provide near-real-time feedback for intraoperative decision-making[68], with SRS having some advantages over CARS, including a linear relationship between signal intensity and chemical concentration. Furthermore, image contrast in CARS is limited by the presence of a non-resonant background signal that interferes with the resonant signals of Raman peaks[69]. Multiple studies have used SRS for the assessment of fresh tissue biopsies from patients with glioblastoma[70,71], with encouraging results. For example, there can be almost perfect inter-observer agreement between H&E-simulating SRS image processing (known as stimulated Raman histology), and conventional H&E staining for discriminating fresh glioblastoma and non-tumour tissue samples[70,71]. Moreover, SRS can show near-perfect concordance with histopathology for the diagnosis of low-grade and high-grade glioblastoma[70,71]. Intravenously administered surface-enhanced Raman scattering nanoparticles can also provide signal enhancement and high-speed acquisition. However, SRS has been assessed mostly preclinically[72–74]; clinically, it may have the advantage of not needing the complex and expensive ultrashort pulse lasers used in other coherent Raman-based techniques[75].

Mid-infrared optoacoustic microscopy—a recent vibrational-imaging spectral technique based on optoacoustic readings—visualizes optical absorption (rather than scattering). It therefore offers higher sensitivity for the label-free imaging of lipids, proteins and carbohydrates at low laser power and less tissue photodamage[76,77]. However, whether it can achieve sufficiently high contrast and image quality for margin assessment has not yet been assessed.

Fluorescence imaging. Fluorescence imaging relies on contrast generation by endogenous tissue fluorophores or exogenous fluorescent agents. It can take the form of intravital fluorescence microscopy or wide-field macroscopic imaging, and uses fluorescence-sensitive cameras and appropriate filters. In general, fluorescence imaging can visualize contrast under the surface of the tissue. In particular, wide-field macroscopic imaging can detect fluorochromes at depths of a few millimetres, especially in the NIR spectral region (because of lower photon attenuation by tissue[78,79]).

Fluorescence confocal microscopy (FCM), the lateral resolution of which is similar to histopathologically relevant dimensions (about 1 µm), can image tissues at resolutions near the limit of optical diffraction (despite photon scattering), albeit at depths generally smaller than 100 µm (ref. [80]). Confocal microscopy scans tissues with a focused light beam and rejects scattered photons by forcing the detection of light through a pinhole, which allows only light from the focus point to be collected. Because of the need to scan photon beams on the tissue surface to generate an image, FCM generally covers small fields of view (typically less than 1 mm), unless long acquisition times are used. For the examination of tissue ex vivo, either endogenous fluorescence or exogenous fluorescent agents (typically applied on the specimen) can be used. FCM has been used for the analysis of fresh tissue samples in various types of cancer[81–83]. For example, a study of fresh tissue samples with breast, colon or thyroid cancer showed that the malignancies were easily detected by FCM following acridine orange staining[83]. In this case, image reconstruction entailed scanning the tissue serially and stitching overlapping images together. Because a typical tissue surface is at least 30–40 cm^2, this can be a slow process. For example, generating an image from a 4-cm^2 section of fresh breast-cancer tissue took approximately 10 min (ref. [84]). The scanning rate could be improved by using a spinning disc[85] or line scanning[86]. The latter has an important disadvantage in that it has unequal resolution along the imaged plane, which results in undesirable distortion in the images. Also, because the interpretation of the greyscale images generated with FCM substantially differs from the interpretation of conventional histopathology, pathologists would need to be trained in FCM image interpretation[87–89].

In two-photon microscopy (TPM)—a nonlinear microscopy technique that has also been developed for imaging the surfaces of tissue blocks at high resolution[90]—fluorescence excitation occurs through two-photon concurrent absorption[90]. This happens only in well-defined volumes at microscopic resolution because of the requirement of high photon coincidence, which is typically achieved through the high spatial and temporal confinement of the illuminating energy. As the excitation for TPM typically lies in the NIR range, it can provide higher penetration depths than FCM[80]. The efficiency of two-photon absorption is low[80] and it requires high power (and often expensive) femtosecond pulse lasers to create sufficient signal. Thus far, TPM has been used for the margin assessments of fresh rectal and fluorescently stained breast-cancer specimens ex vivo[91,92] with imaging speeds of 5–10 min cm^{-2} and penetration depths as high as 100–130 µm. Multiple studies have concluded that the intraoperative use of TPM should be confined to the assessment of small samples only because a lengthy assessment of the entire tissue surface would be a limiting factor in clinical workflows[91,93].

The increasing demand for three-dimensional imaging for tissue analysis has led to the development of light-sheet fluorescence microscopy (LSFM)[94]. In LSFM, a thin 'selective' light beam illuminates the fluorescently stained tissue and the fluorescence signal is collected in the orthogonal direction. Owing to the availability of tissue-clearing methods for making tissues optically transparent[95,96], LSFM enables, for instance, three-dimensional imaging of virtual sections in intact tumour biopsies (and hence, of tissue much larger than the conventional 4-µm tissue section)[97,98]. The thickness of the virtual section is defined by the diameter of the light beam and the diffractive effects in the sample imaged. One of the first studies of this technique showed that the LSFM images of DRAQ5 and eosin-stained core-needle prostate biopsies (2 cm in length, 1 mm in diameter) were similar to those obtained with

conventional H&E-stained slides[97]. Hence, the accuracy of tumour staging can be higher than that of conventional two-dimensional histology[98]. LSFM achieves faster imaging speeds (larger than 40 $mm^3 min^{-1}$) than confocal microscopy (about 4 $mm^2 min^{-1}$)[86]; however, a comparable imaging speed can be achieved using transmission microscopy[89]. For IPAS purposes, the limiting step for the clinical implementation of LSFM is sample preparation, because tissue clearing is a process that typically requires several hours of tissue treatment. There are efforts to speed up this process[95], as illustrated by a recently launched kit that enables the clearing of biopsies in approximately 2 h (ref. [99]). LSFM studies of breast-cancer and prostate-cancer specimens have shown that margin assessments of freshly excised tissue are feasible without the use of optical-clearing methods[97,100]. LSFM has also been used to image irregular margin surfaces of fresh breast tissue stained with SYBR Gold and ATTO 655 NHS ester to generate a comprehensive image of the inked margin. The images, obtained with an imaging speed of 1.5 $cm^2 min^{-1}$, were similar to those obtained with traditional H&E staining, which indicates the potential of LSFM for use in IPAS[101]. Furthermore, because breast tissue is primarily composed of adipose tissue, which is difficult to freeze for FFS, LSFM might be a realistic alternative for assessing resection margins.

Structured illumination microscopy (SIM) represents an alternative approach to address the photon-scattering problem and to image the tissue surface at microscopic resolutions[102]. In SIM, the in-focus plane of the sample is illuminated through a grid with a sinusoidally varying pattern. The spatial pattern facilitates the retention of light from the modulated focal plane while the light from the out-of-focus planes, which is not modulated, is rejected[102]. To complete the image, it is necessary to phase-step this grid pattern over the sample and to collect a set of three images (at points corresponding to phases at angles of 0, $2\pi/3$ and $4\pi/3$) through a simple correction algorithm. SIM has been developed over the years to include super-resolution techniques[103,104]. Recently, video-rate SIM (VR-SIM) has enabled the imaging of large surface areas. This was achieved with a 4.2-megapixel camera that collected each SIM frame in 30 ms (with ~200 ms between frames). This enabled an imaging rate of 18 megapixels per second, and the imaging of the surface area of a resected organ with a lateral resolution of 1.3 μm (refs. [105,106]). VR-SIM also enabled the assessment of the margins of prostatectomy resections stained with acridine orange within 1 h (ref. [105]).

Microscopy with ultraviolet surface excitation (MUSE) is a camera-based technique that illuminates tissue with ultraviolet light[107], typically with wavelengths of less than 300 nm. As the light at these wavelengths is strongly absorbed by proteins within human tissue, the imaging depth is limited to a few micrometres[108]. Hence, because of the absence of out-of-focus signals originating from deeper tissue layers, MUSE can obtain high-contrast images with subcellular resolution. MUSE uses a variety of fluorescent dyes applied ex vivo that can be excited with ultraviolet light and emit photons across the visible spectrum. Although MUSE can be cost-effective[107,109], the costs of the optical components needed for imaging at wavelengths lower than 300 nm can be high (because they do not use the standard quartz typically used in lenses). MUSE methodology for margin assessment is easy to implement in clinical settings, yet only a few pathology-imaging studies have been carried out so far[107,109]. In one such study, fresh tissue biopsies of 15 × 15 mm were stained with SYBR Gold and ATTO 655 NHS ester within 5 min, and the imaging procedure itself took only 2–3 min. Images mimicking H&E histology with a resolution less than 1 μm were obtained using a virtual H&E-rendering algorithm, with a concordance rate between the MUSE images and the conventional H&E images of 93%. Furthermore, the MUSE images showed fewer artefacts than FFS analysis, and allowed for more accurate diagnoses[109]. However, there were several disparities, which were attributed to the thicker sections (10–20 μm), as well as to artefacts caused by irregular surface topology. In this respect, tissue-flattening methods can minimize unintended artefacts and improve image quality.

Wide-field fluorescence imaging is a well-established method in surgical oncology[110]. Since fluorescein was first used 70 years ago to differentiate between tumour and healthy tissue, multiple intravenously administered fluorescent agents have been used for fluorescence-guided surgery. The US Food and Drug Administration approved 5-aminolevulinic acid in 2017 for the detection of tumours in brain surgery[111]. During the past decade, interest has shifted towards tumour-specific fluorescence-imaging agents targeting biomarkers of cancer[22], especially those that emit in the NIR spectrum[79]. Ex vivo wide-field fluorescence imaging of surgical specimens, known as wide-field macroscopic fluorescence imaging (WMFI), uses closed-field imaging systems. Because the environment is easily controllable, this provides more consistent data for margin assessment. Multiple pilot studies have shown that WMFI of intravenously administered targeted fluorescent agents (such as VEGF-A[18,112,113], EGFR[114,115] and PARP1 (ref. [116])) on freshly excised specimens can assist intraoperative margin assessment. The interpretation of the fluorescence images is straightforward because of the heavily surface-weighted signal. Therefore, WMFI can be easily used to map the surgical specimen with a single image, and any areas that are at risk of a close margin are immediately evident. WMFI is faster than conventional histopathological approaches[112,117]. However, its spatial resolution degrades to about 1 mm for the assessment of margins at depths of several millimetres[28]. For example, the surgical specimen could be 'bread-loaf' sliced in the operating room, and the tissue slices imaged to more accurately assess the margins. However, a limitation of WMFI is that the data do not merely reflect the concentration of the fluorescent agent itself, as the imaging results also depend on the type of tissue and on the specific detection equipment and methodology used (that is, the cameras and the specific data-processing techniques). Before WMFI can be implemented clinically, these imaging factors would need to be standardized[21,23,112]. Another logistical challenge is the need to administer the contrast agent up to several days before surgery; this is the case with targeting moieties such as antibody–fluorophore conjugates.

Structural imaging. Optical coherence tomography (OCT)—a mainstream retinal-imaging modality[93]—is a cross-sectional imaging technique that yields images of tissue morphology by registering light that is reflected within tissue[118,119]. OCT is therefore analogous to ultrasound imaging, yet achieves adequate optical resolution at depths from 1 mm to several millimetres (depending on the amount of scattering in the imaged tissue). Typically, the resolution of OCT is between 10 and 30 μm. Intraoperative margin assessment by OCT has been explored in surgical specimens of breast cancer[120–122], renal cancer[123] and oral cancer[124]. However, studies have shown varying results in margin-assessment sensitivity (19–81%) and specificity (56–94%). Also, accuracy is generally lower with increasing depth[124,125], which hampers the dissemination of this technology for use in intraoperative pathology[126].

Second-harmonic generation (SHG) microscopy and third-harmonic generation (THG) microscopy are nonlinear microscopy techniques that obtain structural information on biological specimens. For contrast generation, SHG and THG microscopies take advantage of higher-order light–tissue interactions involving multiple photons[80] and typically use light in the NIR range. They require the formation of a short-lived or virtual energy state[127] rather than actual multiphoton absorption. This type of light–tissue interaction also requires high photon coincidence and therefore high spatiotemporal confinement of the illuminating energy. Similar to TPM, the efficiency of this multiphoton process is low[80], and hence high-power femtosecond pulse lasers are required

to create a sufficiently strong signal. Recently, the use of SHG and THG microscopies has been explored for rapid label-free pathology analyses of freshly excised brain and breast tissues[128,129] (and, when used in combination, they can yield morphological information). However, whether these techniques can distinguish cancerous breast tissue from healthy breast tissue in clinical practice has not yet been studied[129]. Also, the scan speed would need to be greatly improved, as scanning 1 cm^2 of tissue at current speeds would take approximately 3 h.

Optoacoustic imaging. Optoacoustic (or photoacoustic) imaging is increasingly being considered for medical applications. The method detects ultrasound waves emitted as a result of thermoelastic expansion when endogenous or exogenous chromophores absorb delivered pulses of laser light. Because tissue scatters ultrasound less than it scatters light[130], optoacoustic imaging provides higher resolution at greater imaging depths than other optical imaging methods. Optoacoustic imaging can be implemented in the macroscopy, mesoscopy or microscopy domains[28], which in aggregate cover a wide range of biological length-scales[131]. Optoacoustic macroscopy usually attains imaging depths of several centimetres in tissue at 200–300 μm resolution[130–132]. Optoacoustic mesoscopy provides imaging depths of several millimetres with a resolution in the order of tens of micrometres[27]. Optoacoustic microscopy provides even shallower images, yet at resolutions of at least a few micrometres. Optoacoustic mesoscopy and optoacoustic microscopy are better suited for the ex vivo assessment of tumour tissue (dedicated studies of such assessments have yet to be published).

To date, the most common photoabsorbers studied in clinical trials are oxyhaemoglobin and deoxyhaemoglobin, which enable the visualization of microvascular structures to reveal tissue hypoxia or inflammation (through the quantification of signals from haemoglobin as well as oxygen saturation[130,132–135]). Melanin can be used as the endogenous source of contrast to optoacoustically detect lymph-node metastasis in melanomas[33,136,137]. Because endogenous contrast only resolves a limited range of biological processes, most applications of optoacoustic imaging would need the intravenous administration of contrast agents (preferably with high-absorption cross-sections and low fluorescence quantum yields[39,138]). However, contrast agents have not yet been used in real-time intraoperative pathology[139].

Pre-operative radiology

In oncology, CT, MRI and ultrasound are mainly used for diagnostic workup and pre-operative imaging to determine tumour stage. Although these pre-operative three-dimensional images can be interpreted by the surgeon, they are not used to provide real-time feedback during surgery. However, advances in technology should help bring these imaging modalities into the operating room.

The use of radiology for pathological assessments of surgical specimens has increasingly been investigated. This is particularly the case for micro-CT for margin assessment in freshly resected breast-cancer specimens[140–142]. With respect to CT for pre-operative imaging, micro-CT has higher resolution and scans the surgical specimen from multiple angles to provide a three-dimensional image that can be used for margin assessment in all directions. In fact, micro-CT was used for margin assessment with a negative predictive value of 83–95% when imaging the complete surgical specimen within 15 min, although at the modest sensitivities of 56–60%[141,143].

The use of MRI for intraoperative margin assessment has been scarcely investigated. Most studies have focused on correlating pre-operative imaging with post-operative pathology, although some studies reported the use of MRI for margin assessment of freshly resected specimens[144–147]. In general, these studies concluded that MRI is not sufficiently sensitive for the detection of microscopic disease; one study reported a failure to assess margins ex vivo[144], and several studies reported that imaging the entire surgical specimen required more than 1 h (refs. [145,146,148]), which is too long for intraoperative use and decision-making. Also, the intraoperative use of MRI has serious drawbacks; most prominently, high cost and logistical restrictions associated with the size of the instrument (larger for higher resolutions). Such challenges hinder the implementation of MRI in the operating room.

Ultrasound for margin assessment has been used to assess freshly excised kidneys and has been shown to ensure negative margins during partial or complete nephrectomy, with a reported specificity of 100%[149]. Despite meeting the required clinical microscopic margin assessment levels, its low resolution constrains the use of ultrasound for assessments of gross macroscopic margin involvement. Still, advances in high-frequency ultrasound detectors may increase its clinical value.

Conventional radiological imaging techniques are important for pre-operative surgical planning, yet their resolution is in the cubic-millimetre range and hence much lower than the 1–100-μm resolution range offered by optical and optoacoustic imaging techniques. Therefore, they do not meet the spatial resolutions needed to assess tumour margins. Moreover, the use of these techniques in the operating room may be constrained by high costs and by logistics associated with equipment size and operational complexity.

Expected benefits of imaging in IPAS

In this section, we describe the potential implementation of various types of IPAS using three typical clinical workflows as cases. The specific advantages and disadvantages of each imaging technique are listed in Table 2.

Intraoperative lymph-node assessment. The presence of cancer cells in lymph nodes has an important impact on disease-specific survival in the majority of cancer types[30,150,151]. A distinction can be made between macrometastases and micrometastases, and even isolated tumour cells, on the basis of the tumour volume within the lymph node. The presence of macrometastasis in lymph nodes requires further treatment, which generally consists of surgical lymph-node dissection or adjuvant systemic chemotherapy (or both). Further treatment is not often required for isolated tumour cells and micrometastases.

When no reliable histology about lymph-node status is available before surgery, a sentinel-lymph-node biopsy or FFS is performed. In a sentinel-lymph-node biopsy, the first lymph node(s) draining the tumour are collected for diagnostic purposes, as they are representative of the remaining regional lymph nodes[152]. The final histopathological results can take up to 5 working days, and the detection of micrometastasis or isolated tumour cells can take up to 7 days. If metastases are present, a subsequent lymph-node dissection is performed in most cases (in particular, for breast cancer and head-and-neck cancer). Performing this dissection in a second surgery may lead to major consequences in terms of patient discomfort, surgical complications and increased healthcare costs, and in some cases it may not be feasible owing to altered anatomy[5].

Replacing a traditional sentinel-lymph-node biopsy with intraoperative lymph-node assessment requires a high-resolution technique, mainly because the volume of micrometastases can be less than 2 mm^3. The lymph-node samples do not usually exceed 1–2 cm^3 (refs. [3,153]), and hence high imaging speeds are not necessary. Raster scanning the complete lymph node with Raman-based techniques could potentially be used for this purpose. In the future, LSFM after rapid (within minutes) tissue clearance could be employed to assess entire lymph nodes. However, the tissue-clearance process should become more efficient and faster before adequate clinical implementation can be considered. Immediate analysis of the excised lymph node would enable

Table 2 | Characteristics of IPAS according to imaging modality

Imaging modality	Advantages	Disadvantages	Analysis of a selected area or a whole specimen
Spectroscopy imaging			
HSI	Label-free High imaging speed	Costs Complexity	Whole specimen
Raman	Label-free Chemical information Quantitative	Weak intrinsic signal Spot-based Low imaging speed	Selected area[a]
Coherent Raman	Label-free Chemical information High spatial resolution Quantitative	Spot-based Low imaging speed Costs	Selected area[a]
Mid-infrared optoacoustic microscopy	High sensitivity and specificity High contrast	Low imaging speed Preclinical phase	Selected area[a]
Fluorescence imaging			
FCM	High spatial resolution Image mosaicking	Limited imaging depth Spot-based Low imaging speed	Selected area[a]
TPM	High spatial resolution High sensitivity and specificity	Phototoxicity Costs Spot-based Low imaging speed	Selected area[a]
LSFM	High spatial resolution High sensitivity and specificity	Limited imaging depth	Selected area[a]
SIM	High spatial resolution	Limited imaging depth Low imaging speed	Selected area[a]
MUSE	High spatial resolution High imaging speed	Limited imaging depth	Selected area[a]
Wide-field fluorescence	Real-time imaging Large scan area High sensitivity	Surface-weighted signal Semiquantitative Interference of optical parameters	Whole specimen
Structural imaging			
OCT	Label-free High resolution	Limited contrast Small scan area Requires training for reading	Selected area
SHG and THG microscopies	Label-free High sensitivity	Limited imaging depth Low imaging speed	Selected area[a]
Optoacoustic imaging			
Mesoscopy	High imaging speed Penetration depth High sensitivity	No clinical contrast agents available Semi-quantitative	Selected area
Microscopy	High resolution Scalable	Low imaging speed	Selected area
Radiology			
CT	Unlimited penetration depth Large scan area	Limited contrast No biochemical information Limited resolution	Whole specimen
MRI	Unlimited penetration depth High soft tissue contrast Large scan area	Cost Low sensitivity Low imaging speed	Whole specimen
Ultrasound	Real-time Large scan area	Limited resolution Limited contrast agents Low sensitivity	Whole specimen

An overview of the clinical advantages and disadvantages of IPAS with respect to their intraoperative implementation. [a]Unless tissue clearing is used, this technique can only be applied to tumour types for which a tumour-positive margin is defined as ink on tumour (Table 1).

additional lymph-node dissection during the same surgical procedure and would eliminate the need for a second surgery (Fig. 2). In view of the percentage of tumour-positive sentinel-lymph-node biopsies that are detected after initial surgeries (7–50%[154]), such real-time information could boost the efficiency and lessen the cost of these surgical procedures.

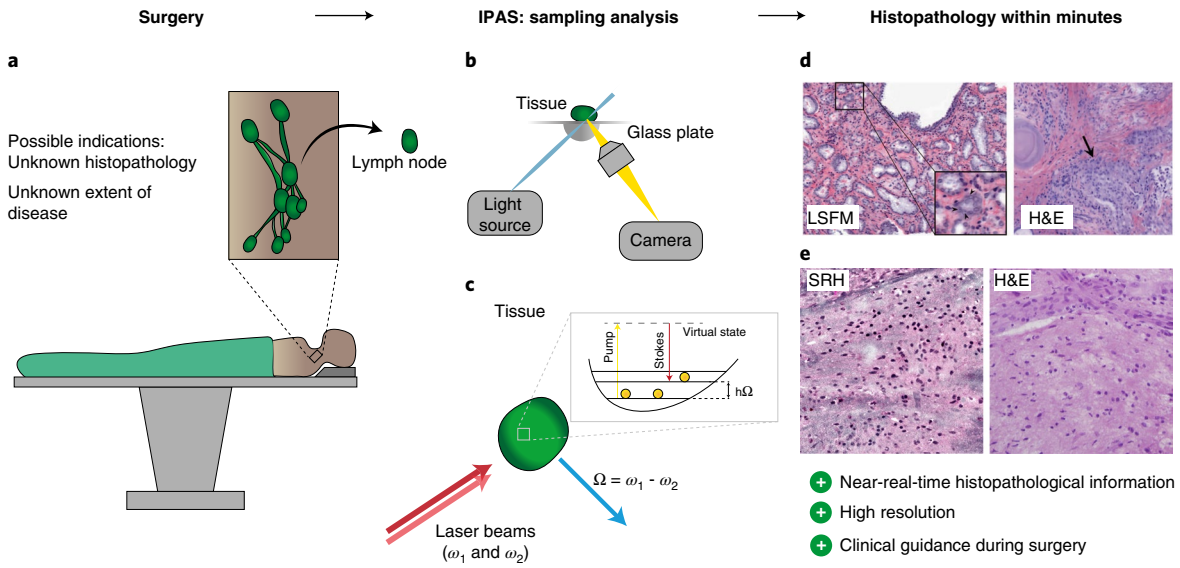

Fig. 2 | Flowchart for small-tissue analysis by IPAS. The intraoperative assessment of small tissue biopsies may enhance clinical decision-making during surgery. **a**, A single lymph node is excised to determine whether additional lymph-node dissection is necessary. **b**,**c**, Examples of imaging techniques, such as LSFM (**b**) and SRS spectroscopy (**c**), suitable for IPAS. **d**,**e**, Representative examples of LSFM[100] (**d**) and stimulated Raman histology (SRH)[71] (**e**) images showing good correlation with conventional H&E-stained sections. Figure adapted with permission from: **d**, ref. [100], College of American Pathologists; **e**, ref. [71], Springer Nature Limited.

Intraoperative margin assessment in breast-cancer surgery. To ensure a negative margin across various solid tumour types, surgical subspecialties use different surgical resection metrics. In some cases, there is no clear consensus (Tables 1 and 2). In the case of stage I/II breast cancers, guidelines from the American Society of Clinical Oncology and Cancer Care Ontario state that 'no ink on tumour' (that is, no tumour at the outer edge of the tissue) at the surgical resection margin can be considered as a tumour-negative margin[5]. This consideration also applies to many other tumour types (Table 1).

The optimal IPAS technique for tumour types for which a tumour-negative margin is defined as no ink on tumour does not require great imaging depth because assessment of the first cell layers is sufficient. Indeed, at a certain penetration depth, no discrimination can be made between superficial and deep signals, which leads to increased false positives. Moreover, a large field of view needs to be available for the rapid evaluation of all the resection margins.

Among the potential IPAS techniques, MUSE has been shown to be reliable for the rapid margin assessment of lumpectomy specimens. However, specimens with a greater volume require faster image-acquisition rates than MUSE provides. Wide-field fluorescence imaging could be promising in this regard. However, because it does not allow for signal quantification or microscopic confirmation, fluorescence-guided imaging should be restricted to red-flag detection (that is, to sample screening for the identification of suspicious areas). Further evaluation of the red-flagged areas should then be performed with a suitable imaging technique. Positive margins are reported in up to 40% of breast-cancer and prostate-cancer surgery procedures[155–157], and hence confirming tumour-negative surgical margins can prevent adjuvant re-excision surgery. This underscores the urgent need for technological advancements in image-guided intraoperative tumour detection (Fig. 3).

Intraoperative margin assessment in surgery for head-and-neck cancer. The real-world challenges posed by margin assessment during surgery are particularly illustrated by the frequent intraoperative consultations with the pathologist that occur during head-and-neck cancer surgery[12]. The aim of surgical resection should be to obtain a margin larger than 5 mm on the histopathological slides[158,159]. When the margin is between 1 and 5 mm, it is defined as a close margin; a positive margin is defined as tumour cells within 1 mm of the surgical margin[160]. Consequently, in head-and-neck cancer, an IPAS technique is required to analyse the complete specimen rapidly (within minutes) to a depth of up to 5 mm. Wide-field fluorescence imaging would seem an attractive option for this purpose, as considerable clinical experience has been gained over the past decade[114,161]. As with margin assessment in breast-cancer surgery, subsequent analysis of the margin of the highly fluorescent area(s) could be performed via a high-resolution technique. Because of the necessity of a penetration depth of at least 5 mm, mesoscopic optoacoustic imaging might be an alternative to wide-field fluorescence imaging for the assessment of the margins of freshly excised surgical specimens; however, no clinical studies support its use yet. For adequate clinical use, the current imaging speed of about 6 $cm^2 min^{-1}$ should improve by at least one order of magnitude, and dedicated optoacoustic contrast agents would be needed for tumour-specific imaging.

Head-and-neck-cancer surgery is performed in anatomically delicate areas with high functional demands. The common practice is, therefore, to perform immediate reconstruction to restore functionality. The consequence of such direct reconstruction is that no second surgery is possible. As a result, many patients with tumour-positive margins (up to 23%) are treated post-operatively with radiation or chemoradiation therapy, which entails severe comorbidities[14,162,163]. Intraoperative detection of tumour-positive margins with IPAS would enable immediate adjustments and prevent major burdens associated with post-operative treatment[14,162,163].

Outlook

Tumour-positive margins are an unwanted post-surgical outcome in many cases[1]. Imaging techniques that can selectively and accurately detect cancers intraoperatively—in particular, tumour-positive margins, occult tumours and tumour-positive lymph nodes—will

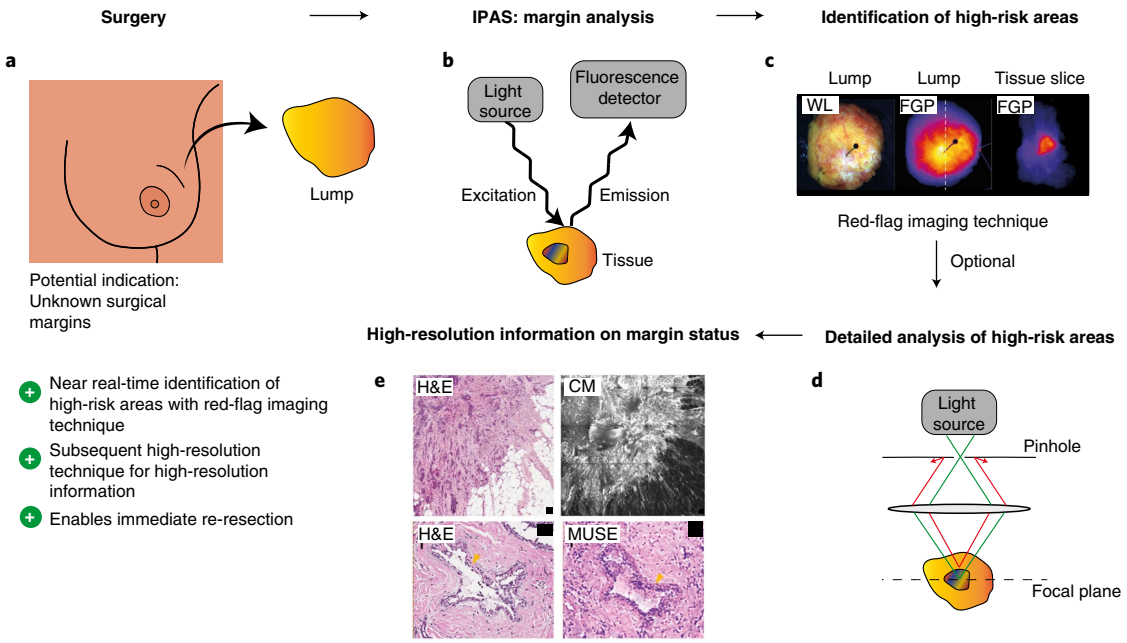

Fig. 3 | Flowchart for margin assessment by IPAS. Intraoperative margin assessment by IPAS may facilitate immediate re-intervention, thereby reducing the need for adjuvant therapy or re-excision surgery. An IPAS technique that enables rapid scanning of a large field of view could identify areas at risk. If necessary, a high-resolution IPAS technique can then be used for the detailed analysis of a small area on the surface. **a**, A lump is excised during breast-cancer surgery. **b**, Fluorescence-guided imaging is suitable for IPAS. **c**, Representative examples of WMFI of a freshly excised lump[112]. FGP, fluorescence-guided pathology. **d**, Confocal microscopy may enable high-resolution imaging. **e**, Representative examples of CM[83] and MUSE[109] images showing good correlation with conventional H&E-stained sections. Yellow arrowheads indicate ductal carcinoma in situ. WL, white light. Figure adapted with permission from: **c**, ref. [112], Springer Nature Limited; **e**, ref. [83], United States & Canadian Academy of Pathology (top row); ref. [109] under a Creative Commons CC BY 4.0 license (bottom row).

improve surgery outcomes and ultimately survival rates. Several imaging techniques could in principle enhance the detection of a broad range of tumour types before and during surgery. However, most clinical studies and improvements have focused mainly on in situ tumour detection, and relatively few studies have been carried out on imaging-assisted assessments of the specimen immediately after excision. Incorporating IPAS in clinical workflows for the assessment of surgical specimens would open up new possibilities in the pathological assessment of excised tissue. Further research in imaging techniques for enhanced tumour detection during surgery are therefore highly needed.

Adequate clinical implementation of IPAS techniques would require consideration of several technical and clinical factors. The following key technical requirements would need improvements: image resolution, penetration depth, field of view, and acquisition time. These factors can be prioritized differently depending on the specific clinical indication. For tissue biopsies, we rank image resolution and sensitivity as the most important features for IPAS. In contrast, whole surgical specimens require large fields of view and high imaging speeds; a complimentary high-resolution technique can then be used to assess the highlighted areas in more detail (however, the necessary penetration depth might differ across tumour types; Table 1).

The clinical implementation of IPAS will require rigorous and standardized pre-operative planning. A first step would be to determine whether endogenous contrast is sufficient or whether exogenous (targeted) contrast agents are required. Although endogenous contrast is favourable in terms of patient safety, costs and logistics, the use of exogenous contrast agents in IPAS might generate better contrast and enhance tumour specificity. This trade-off should be investigated. Regardless, and most importantly for clinicians, the imaging technique should be user-friendly, and easy and fast to implement.

Clinical trials assessing IPAS should be designed to provide clinical evidence of whether there is added value for clinicians, such as tumour-negative surgical margins and enhanced tumour detection that assist decision-making. Lessons could be learned from the image-guided surgery techniques that were at the same point of development about a decade ago[15] and that are currently being assessed in phase II and phase III clinical studies[111]. Most importantly, the gaps between technical challenges and clinical needs will need to be bridged.

Received: 1 May 2019; Accepted: 17 June 2021;
Published online: 8 November 2021

References

1. Orosco, R. K. et al. Positive surgical margins in the 10 most common solid cancers. *Sci. Rep.* **8**, 56–86 (2018).
2. Sutton, D. N., Brown, J. S., Rogers, S. N., Vaughan, E. D. & Woolgar, J. A. The prognostic implications of the surgical margin in oral squamous cell carcinoma. *Int. J. Oral. Maxillofac. Surg.* **32**, 30–34 (2003).
3. Binahmed, A., Nason, R. W. & Abdoh, A. A. The clinical significance of the positive surgical margin in oral cancer. *Oral Oncol.* **43**, 780–784 (2007).
4. Meric, F. et al. Positive surgical margins and ipsilateral breast tumour recurrence predict disease-specific survival after breast-conserving therapy. *Cancer* **97**, 926–933 (2003).
5. Moran, M. S. et al. Society of Surgical Oncology–American Society for Radiation Oncology consensus guideline on margins for breast-conserving surgery with whole-breast irradiation in stages I and II invasive breast cancer. *Int. J. Radiat. Oncol. Biol. Phys.* **88**, 553–564 (2014).
6. Peeters, K. C. M. J. et al. The TME trial after a median follow-up of 6 years: increased local control but no survival benefit in irradiated patients with resectable rectal carcinoma. *Ann. Surg.* **246**, 693–701 (2007).
7. Lin, H.-H. et al. Circumferential margin plays an independent impact on the outcome of rectal cancer patients receiving curative total mesorectal excision. *Am. J. Surg.* **206**, 771–777 (2013).
8. Sasikumar, A., Bhan, C., Jenkins, J. T., Antoniou, A. & Murphy, J. Systematic review of pelvic exenteration with en bloc sacrectomy for recurrent rectal adenocarcinoma: R0 resection predicts disease-free survival. *Dis. Colon Rectum* **60**, 346–352 (2017).

9. Crane, L. M. A. et al. Intraoperative imaging in ovarian cancer: fact or fiction? *Mol. Imaging* **10**, 248–257 (2011).
10. Pop, C.-F. et al. Ex vivo indocyanine green fluorescence imaging for the detection of lymph node involvement in advanced-stage ovarian cancer. *J. Surg. Oncol.* **118**, 1163–1169 (2018).
11. Chambers, K. J., Kraft, S. & Emerick, K. Evaluation of frozen section margins in high-risk cutaneous squamous cell carcinomas of the head and neck. *Laryngoscope* **125**, 636–639 (2015).
12. Mahe, E. et al. Intraoperative pathology consultation: error, cause and impact. *Can. J. Surg.* **56**, E13–E18 (2013).
13. Helliwell, T. R & Woolgar, J. A. *Standards and Datasets for Reporting Cancers. Dataset for Histopathology Reporting of Mucosal Malignancies of the Oral Cavity* (The Royal College of Pathologists, 2013).
14. Woolgar, J. A. & Triantafyllou, A. A histopathological appraisal of surgical margins in oral and oropharyngeal cancer resection specimens. *Oral Oncol.* **41**, 1034–1043 (2005).
15. van Dam, G. M. et al. Intraoperative tumour-specific fluorescence imaging in ovarian cancer by folate receptor-α targeting: first in-human results. *Nat. Med.* **17**, 1315–1319 (2011).
16. Vahrmeijer, A. L., Hutteman, M., van der Vorst, J. R., van de Velde, C. J. H. & Frangioni, J. V. Image-guided cancer surgery using near-infrared fluorescence. *Nat. Rev. Clin. Oncol.* **10**, 507–518 (2013).
17. de Boer, E. et al. In vivo fluorescence immunohistochemistry: localization of fluorescently labeled cetuximab in squamous cell carcinomas. *Sci. Rep.* **5**, 14 (2015).
18. Harlaar, N. J. et al. Molecular fluorescence-guided surgery of peritoneal carcinomatosis of colorectal origin: a single-centre feasibility study. *Lancet Gastroenterol. Hepatol.* **1**, 283–290 (2016).
19. Moore, L. S. et al. Effects of an unlabeled loading dose on tumour-specific uptake of a fluorescently labeled antibody for optical surgical navigation. *Mol. Imaging Biol.* **19**, 610–616 (2016).
20. Diot, G. et al. Multispectral optoacoustic tomography (MSOT) of human breast cancer. *Clin. Cancer Res.* **23**, 6912–6922 (2017).
21. Koch, M., Symvoulidis, P. & Ntziachristos, V. Tackling standardization in fluorescence molecular imaging. *Nat. Photon.* **12**, 505–515 (2018).
22. Koch, M. & Ntziachristos, V. Advancing surgical vision with fluorescence imaging. *Annu. Rev. Med.* **67**, 153–164 (2016).
23. Gorpas, D. et al. Multi-parametric standardization of fluorescence imaging systems based on a composite phantom. *IEEE Trans. Biomed. Eng.* **67**, 185–192 (2020).
24. Weissleder, R. & Nahrendorf, M. Advancing biomedical imaging. *Proc. Natl Acad. Sci. USA* **112**, 14424–14428 (2015).
25. Thakor, A. S. & Gambhir, S. S. Nanooncology: the future of cancer diagnosis and therapy. *CA Cancer J. Clin.* **63**, 395–418 (2013).
26. Taruttis, A., van Dam, G. M. & Ntziachristos, V. Mesoscopic and macroscopic optoacoustic imaging of cancer. *Cancer Res.* **75**, 1548–1559 (2015).
27. Omar, M., Aguirre, J. & Ntziachristos, V. Optoacoustic mesoscopy for biomedicine. *Nat. Biomed. Eng.* **3**, 354–370 (2019).
28. Ntziachristos, V. Going deeper than microscopy: the optical imaging frontier in biology. *Nat. Meth.* **7**, 603–614 (2010).
29. Lauwerends, L. J. et al. Real-time fluorescence imaging in intraoperative decision making for cancer surgery. *Lancet Oncol.* **22**, e186–e195 (2021).
30. Sloothaak, D. A. M. et al. Prognostic implications of occult nodal tumour cells in stage I and II colon cancer: the correlation between micrometastasis and disease recurrence. *Eur. J. Surg. Oncol.* **43**, 1456–1462 (2017).
31. de Boer, E. et al. Optical innovations in surgery. *Br. J. Surg.* **102**, e56–e72 (2015).
32. Nagengast, W. B. et al. Near-infrared fluorescence molecular endoscopy detects dysplastic oesophageal lesions using topical and systemic tracer of vascular endothelial growth factor A. *Gut* **68**, 7–10 (2019).
33. Stoffels, I. et al. Metastatic status of sentinel lymph nodes in melanoma determined noninvasively with multispectral optoacoustic imaging. *Sci. Transl. Med.* **7**, 317ra199 (2015).
34. Ntziachristos, V., Pleitez, M. A., Aime, S. & Brindle, K. M. Emerging technologies to image tissue metabolism. *Cell Metab.* **29**, 518–538 (2019).
35. Boezeman, R. P. E., Moll, F. L., Unlu, C. & de Vries, J.-P. P. M. Systematic review of clinical applications of monitoring muscle tissue oxygenation with near-infrared spectroscopy in vascular disease. *Microvasc. Res.* **104**, 11–22 (2016).
36. Boamfa, M. I. et al. Combined transmission, dark field and fluorescence microscopy for intact, 3D tissue analysis of biopsies. *J. Biomed. Opt.* **25**, 116503 (2020).
37. Regensburger, A. P. et al. Detection of collagens by multispectral optoacoustic tomography as an imaging biomarker for Duchenne muscular dystrophy. *Nat. Med.* **25**, 1905–1915 (2019).
38. Bourantas, C. V. et al. Hybrid intravascular imaging: recent advances, technical considerations, and current applications in the study of plaque pathophysiology. *Eur. Heart J.* **38**, 400–412 (2017).
39. Weber, J., Beard, P. C. & Bohndiek, S. E. Contrast agents for molecular photoacoustic imaging. *Nat. Meth.* **13**, 639–650 (2016).
40. Fu, Q., Zhu, R., Song, J., Yang, H. & Chen, X. Photoacoustic Imaging: contrast agents and their biomedical applications. *Adv. Mater.* **31**, e1805875 (2019).
41. Bremer, C., Ntziachristos, V. & Weissleder, R. Optical-based molecular imaging: contrast agents and potential medical applications. *Eur. Radiol.* **13**, 231–243 (2003).
42. Burggraaf, J. et al. Detection of colorectal polyps in humans using an intravenously administered fluorescent peptide targeted against c-Met. *Nat. Med.* **21**, 955–961 (2015).
43. Allegra, A. et al. Nanobodies and cancer: current status and new perspectives. *Cancer Invest.* **36**, 221–237 (2018).
44. Wei, Y. et al. Biocompatible low-retention superparamagnetic iron oxide nanoclusters as contrast agents for magnetic resonance imaging of liver tumour. *J. Biomed. Nanotechnol.* **11**, 854–864 (2015).
45. Zhao, T. et al. A transistor-like pH nanoprobe for tumour detection and image-guided surgery. *Nat. Biomed. Eng.* **1**, 0006 (2016).
46. Liu, Q. Role of optical spectroscopy using endogenous contrasts in clinical cancer diagnosis. *World J. Clin. Oncol.* **2**, 50–63 (2011).
47. Goetz, A. F. H. Three decades of hyperspectral remote sensing of the Earth: a personal view. *Remote Sens. Environ.* **113**, s1–s16 (2009).
48. Lu, G. & Fei, B. Medical hyperspectral imaging: a review. *J. Biomed. Opt.* **19**, 10901 (2014).
49. Boas, D. A, Pitris, C & Ramanujam, N. *Handbook of Biomedical Optics* (CRC Press, 2011).
50. Fei, B. et al. Label-free reflectance hyperspectral imaging for tumour margin assessment: a pilot study on surgical specimens of cancer patients. *J. Biomed. Opt.* **22**, 1–7 (2017).
51. Fei, B. et al. Label-free hyperspectral imaging and quantification methods for surgical margin assessment of tissue specimens of cancer patients. *Annu. Int. Conf. IEEE Eng. Med. Biol. Soc.* **2017**, 4041–4045 (2017).
52. Fei, B. et al. Tumour margin assessment of surgical tissue specimen of cancer patients using label-free hyperspectral imaging. *Proc. SPIE Int. Soc. Opt. Eng.* **10054**, 100540E (2017).
53. Halicek, et al.Tumour margin classification of head and neck cancer using hyperspectral imaging and convolutional neural networks. *Proc. SPIE Int. Soc. Opt. Eng.* **10576**, 1057605 (2018).
54. Lu, G. et al. Detection of head and neck cancer in surgical specimens using quantitative hyperspectral imaging. *Clin. Cancer Res.* **23**, 5426–5436 (2017).
55. Baltussen, E. J. M. et al. Hyperspectral imaging for tissue classification, a way toward smart laparoscopic colorectal surgery. *J. Biomed. Opt.* **24**, 1–9 (2019).
56. Brouwer de Koning, S. G. et al. Toward assessment of resection margins using hyperspectral diffuse reflection imaging (400–1,700 nm) during tongue cancer surgery. *Lasers Surg. Med.* **52**, 496–502 (2020).
57. Kho, E. et al. Imaging depth variations in hyperspectral imaging: development of a method to detect tumour up to the required tumour-free margin width. *J. Biophotonics* **12**, e201900086 (2019).
58. Kho, E. et al. Hyperspectral imaging for resection margin assessment during cancer surgery. *Clin. Cancer Res.* **25**, 3572–3580 (2019).
59. Long, D. A. *Raman Spectroscopy* (McGraw-Hill, 1977).
60. Barroso, E. M. et al. Raman spectroscopy for assessment of bone resection margins in mandibulectomy for oral cavity squamous cell carcinoma. *Eur. J. Cancer* **92**, 77–87 (2018).
61. Barroso, E. M. et al. Water concentration analysis by Raman spectroscopy to determine the location of the tumour border in oral cancer surgery. *Cancer Res.* **76**, 5945–5953 (2016).
62. Cals, F. L. J. et al. Development and validation of Raman spectroscopic classification models to discriminate tongue squamous cell carcinoma from non-tumourous tissue. *Oral Oncol.* **60**, 41–47 (2016).
63. Nguyen, J. Q. et al. Intraoperative Raman spectroscopy of soft tissue sarcomas. *Lasers Surg. Med.* **48**, 774–781 (2016).
64. Camp, C. H. J. et al. High-speed coherent Raman fingerprint imaging of biological tissues. *Nat. Photonics* **8**, 627–634 (2014).
65. Byrne, H. J. et al. Spectropathology for the next generation: quo vadis? *Analyst* **140**, 2066–2073 (2015).
66. Evans, C. L. et al. Chemical imaging of tissue in vivo with video-rate coherent anti-Stokes Raman scattering microscopy. *Proc. Natl Acad. Sci. USA* **102**, 16807–16812 (2005).
67. Saar, B. G. et al. Video-rate molecular imaging in vivo with stimulated Raman scattering. *Science* **330**, 1368–1370 (2010).
68. Hollon, T. C. et al. Near real-time intraoperative brain tumour diagnosis using stimulated Raman histology and deep neural networks. *Nat. Med.* **26**, 52–58 (2020).
69. Freudiger, C. W. et al. Label-free biomedical imaging with high sensitivity by stimulated Raman scattering microscopy. *Science* **322**, 1857–1861 (2008).
70. Ji, M. et al. Detection of human brain tumour infiltration with quantitative stimulated Raman scattering microscopy. *Sci. Transl. Med.* **7**, 309ra163 (2015).

71. Orringer, D. A. et al. Rapid intraoperative histology of unprocessed surgical specimens via fibre-laser-based stimulated Raman scattering microscopy. *Nat. Biomed. Eng.* **1**, 0027 (2017).
72. Harmsen, S. et al. Detection of premalignant gastrointestinal lesions using surface-enhanced resonance raman scattering-nanoparticle endoscopy. *ACS Nano* **13**, 1354–1364 (2019).
73. Davis, R. M. et al. Surface-enhanced Raman scattering nanoparticles for multiplexed imaging of bladder cancer tissue permeability and molecular phenotype. *ACS Nano* **12**, 9669–9679 (2018).
74. Arami, H. et al. Nanomedicine for spontaneous brain tumours: a companion clinical trial. *ACS Nano* **13**, 2858–2869 (2019).
75. Meng, Z., Petrov, G. I. & Yakovlev, V. V. Continuous-wave stimulated Raman scattering (cwSRS) microscopy. *Appl. Phys. B* **112**, 99–103 (2013).
76. Pleitez, M. A. et al. Label-free metabolic imaging by mid-infrared optoacoustic microscopy in living cells. *Nat. Biotechnol.* **38**, 293–296 (2020).
77. Strack, R. Mid-IR optoacoustic microscopy. *Nat. Meth.* **17**, 251 (2020).
78. Weissleder, R. & Pittet, M. J. Imaging in the era of molecular oncology. *Nature* **452**, 580–589 (2008).
79. Weissleder, R. & Ntziachristos, V. Shedding light onto live molecular targets. *Nat. Med.* **9**, 123–128 (2003).
80. Helmchen, F. & Denk, W. Deep tissue two-photon microscopy. *Nat. Meth.* **2**, 932–940 (2005).
81. Gareau, D. S. Feasibility of digitally stained multimodal confocal mosaics to simulate histopathology. *J. Biomed. Opt.* **14**, 034050 (2009).
82. Hallani, El,S. et al. Ex vivo confocal imaging with contrast agents for the detection of oral potentially malignant lesions. *Oral Oncol.* **49**, 582–590 (2013).
83. Ragazzi, M. et al. Fluorescence confocal microscopy for pathologists. *Mod. Pathol.* **27**, 460–471 (2014).
84. Abeytunge, S. et al. Evaluation of breast tissue with confocal strip-mosaicking microscopy: a test approach emulating pathology-like examination. *J. Biomed. Opt.* **22**, 34002 (2017).
85. Schueder, F. et al. Multiplexed 3D super-resolution imaging of whole cells using spinning disk confocal microscopy and DNA-PAINT. *Nat. Commun.* **8**, 2090 (2017).
86. van Royen, M. E. et al. Three-dimensional microscopic analysis of clinical prostate specimens. *Histopathology* **69**, 985–992 (2016).
87. Gareau, D. S., Jeon, H., Nehal, K. S. & Rajadhyaksha, M. Rapid screening of cancer margins in tissue with multimodal confocal microscopy. *J. Surg. Res.* **178**, 533–538 (2012).
88. Peters, N., Schubert, M., Metzler, G., Geppert, J.-P. & Moehrle, M. Diagnostic accuracy of a new ex vivo confocal laser scanning microscope compared to H&E-stained paraffin slides for micrographic surgery of basal cell carcinoma. *J. Eur. Acad. Dermatol. Venereol.* **33**, 298–304 (2019).
89. Bini, J. et al. Confocal mosaicing microscopy of human skin ex vivo: spectral analysis for digital staining to simulate histology-like appearance. *J. Biomed. Opt.* **16**, 076008 (2011).
90. Denk, W., Strickler, J. H. & Webb, W. W. Two-photon laser scanning fluorescence microscopy. *Science* **248**, 73–76 (1990).
91. Yan, J. et al. Real-time optical diagnosis for surgical margin in low rectal cancer using multiphoton microscopy. *Surg. Endosc.* **28**, 36–41 (2014).
92. Cahill, L. C. et al. Rapid virtual hematoxylin and eosin histology of breast tissue specimens using a compact fluorescence nonlinear microscope. *Lab Invest.* **98**, 150–160 (2018).
93. Schmidt-Erfurth, U., Klimscha, S., Waldstein, S. M. & Bogunovic, H. A view of the current and future role of optical coherence tomography in the management of age-related macular degeneration. *Eye (Lond.)* **31**, 26–44 (2017).
94. Huisken, J., Swoger, J., Del Bene, F., Wittbrodt, J. & Stelzer, E. H. K. Optical sectioning deep inside live embryos by selective plane illumination microscopy. *Science* **305**, 1007–1009 (2004).
95. Chung, K. et al. Structural and molecular interrogation of intact biological systems. *Nature* **497**, 332–337 (2013).
96. Erturk, A. et al. Three-dimensional imaging of solvent-cleared organs using 3DISCO. *Nat. Protoc.* **7**, 1983–1995 (2012).
97. Glaser, A. K. et al. Light-sheet microscopy for slide-free non-destructive pathology of large clinical specimens. *Nat. Biomed. Eng.* **1**, 0084 (2017).
98. Tanaka, N. et al. Whole-tissue biopsy phenotyping of three-dimensional tumours reveals patterns of cancer heterogeneity. *Nat. Biomed. Eng.* **1**, 796–806 (2017).
99. Villani, T. S., Koroch, A. R. & Simon, J. E. An improved clearing and mounting solution to replace chloral hydrate in microscopic applications. *Appl. Plant Sci.* **1**, 1300016 (2013).
100. Reder, N. P. et al. Open-top light-sheet microscopy image atlas of prostate core needle biopsies. *Arch. Pathol. Lab. Med.* **143**, 1069–1075 (2019).
101. Chen, Y. et al. Rapid pathology of lumpectomy margins with open-top light-sheet (OTLS) microscopy. *Biomed. Opt. Express* **10**, 1257–1272 (2019).
102. Neill, M. A. A., Juskaitis, R. & Wilson, T. Method of obtaining optical sectioning by using structured light in a conventional microscope. *Opt. Lett.* **22**, 1905–1907 (1997).
103. Mertz, J. Optical sectioning microscopy with planar or structured illumination. *Nat. Meth.* **8**, 811–819 (2011).
104. Wu, Y. & Shroff, H. Faster, sharper, and deeper: structured illumination microscopy for biological imaging. *Nat. Meth.* **15**, 1011–1019 (2018).
105. Wang, M. et al. Gigapixel surface imaging of radical prostatectomy specimens for comprehensive detection of cancer-positive surgical margins using structured illumination microscopy. *Sci. Rep.* **6**, 27419 (2016).
106. Schlichenmeyer, T. C., Wang, M., Elfer, K. N. & Brown, J. Q. Video-rate structured illumination microscopy for high-throughput imaging of large tissue areas. *Biomed. Opt. Express* **5**, 366–12 (2014).
107. Fereidouni, F. et al. Microscopy with ultraviolet surface excitation for rapid slide-free histology. *Nat. Biomed. Eng.* **1**, 957–966 (2017).
108. An, J.-P. et al. R2R3-MYB transcription factor MdMYB23 is involved in the cold tolerance and proanthocyanidin accumulation in apple. *Plant J.* **96**, 562–577 (2018).
109. Xie, W. et al. Microscopy with ultraviolet surface excitation for wide-area pathology of breast surgical margins. *J. Biomed. Opt.* **24**, 1–11 (2019).
110. Moore, G. E. Fluorescein as an agent in the differentiation of normal and malignant tissues. *Science* **106**, 130–131 (1947).
111. Stummer, W. et al. Fluorescence-guided surgery with 5-aminolevulinic acid for resection of malignant glioma: a randomised controlled multicentre phase III trial. *Lancet Oncol.* **7**, 392–401 (2006).
112. Koller, M. et al. Implementation and benchmarking of a novel analytical framework to clinically evaluate tumour-specific fluorescent tracers. *Nat. Commun.* **9**, 37–39 (2018).
113. de Jongh, S. J. et al. Back-table fluorescence-guided imaging for circumferential resection margin evaluation using bevacizumab-800CW in patients with locally advanced rectal cancer. *J. Nucl. Med.* **61**, 655–661 (2020).
114. Rosenthal, E. L. et al. Safety and tumour specificity of cetuximab-IRDye800 for surgical navigation in head and neck cancer. *Clin. Cancer Res.* **21**, 3658–3666 (2015).
115. Voskuil, F. J. et al. Fluorescence-guided imaging for resection margin evaluation in head and neck cancer patients using cetuximab-800CW: a quantitative dose-escalation study. *Theranostics* **10**, 3994–4005 (2020).
116. Kossatz, S. et al. Validation of the use of a fluorescent PARP1 inhibitor for the detection of oral, oropharyngeal and oesophageal epithelial cancers. *Nat. Biomed. Eng.* **4**, 272–285 (2020).
117. van Keulen, S. et al. Rapid, non-invasive fluorescence margin assessment: optical specimen mapping in oral squamous cell carcinoma. *Oral Oncol.* **88**, 58–65 (2019).
118. Huang, D. et al. Optical coherence tomography. *Science* **254**, 1178–1181 (1991).
119. Sainter, A. W., King, T. A. & Dickinson, M. R. Effect of target biological tissue and choice of light source on penetration depth and resolution in optical coherence tomography. *J. Biomed. Opt.* **9**, 193–199 (2004).
120. Zysk, A. M. et al. Intraoperative assessment of final margins with a handheld optical imaging probe during breast-conserving surgery may reduce the reoperation rate: results of a multicenter study. *Ann. Surg. Oncol.* **22**, 3356–3362 (2015).
121. Nguyen, F. T. et al. Intraoperative evaluation of breast tumour margins with optical coherence tomography. *Cancer Res.* **69**, 8790–8796 (2009).
122. Erickson-Bhatt, S. J. et al. Real-time imaging of the resection bed using a handheld probe to reduce incidence of microscopic positive margins in cancer surgery. *Cancer Res.* **75**, 3706–3712 (2015).
123. Ludwig, W. W. et al. Margin assessment in renal surgery using a handheld optical coherence tomography probe. *Urology* **113**, 241–245 (2018).
124. Hamdoon, Z., Jerjes, W., McKenzie, G., Jay, A. & Hopper, C. Optical coherence tomography in the assessment of oral squamous cell carcinoma resection margins. *Photodiagnosis Photodyn. Ther.* **13**, 211–217 (2016).
125. Rashed, D. et al. Rapid ex vivo examination of Mohs specimens using optical coherence tomography. *Photodiagnosis Photodyn. Ther.* **19**, 243–248 (2017).
126. Popescu, D. P. et al. Optical coherence tomography: fundamental principles, instrumental designs and biomedical applications. *Biophys. Rev.* **3**, 155 (2011).
127. Mertz, J. Nonlinear microscopy: new techniques and applications. *Curr. Opin. Neurobiol.* **14**, 610–616 (2004).
128. Kuzmin, N. V. et al. Third harmonic generation imaging for fast, label-free pathology of human brain tumours. *Biomed. Opt. Express* **7**, 1889–1904 (2016).
129. van Huizen, L. M. G. et al. Second and third harmonic generation microscopy visualizes key structural components in fresh unprocessed healthy human breast tissue. *J. Biophotonics* **7**, e201800297 (2019).
130. Duck, F. A. *Physical Properties Of Tissue: A Comprehensive Reference Book* (Academic Press, 1990).
131. Wang, L. V. & Hu, S. Photoacoustic tomography: in vivo imaging from organelles to organs. *Science* **335**, 1458–1462 (2012).
132. Taruttis, A. & Ntziachristos, V. Advances in real-time multispectral optoacoustic imaging and its applications. *Nat. Photon.* **9**, 219–227 (2015).
133. Ntziachristos, V., Ripoll, J., Wang, L. V. & Weissleder, R. Looking and listening to light: the evolution of whole-body photonic imaging. *Nat. Biotechnol.* **23**, 313–320 (2005).

134. Dima, A. & Ntziachristos, V. In-vivo handheld optoacoustic tomography of the human thyroid. *Photoacoustics* **4**, 65–69 (2016).
135. Lin, L. et al. Single-breath-hold photoacoustic computed tomography of the breast. *Nat. Commun.* **9**, 2352 (2018).
136. Zhou, Y. et al. Noninvasive determination of melanoma depth using a handheld photoacoustic probe. *J. Invest. Dermatol.* **137**, 1370–1372 (2017).
137. Kim, J. et al. Multispectral ex vivo photoacoustic imaging of cutaneous melanoma for better selection of the excision margin. *Br. J. Dermatol.* **179**, 780–782 (2018).
138. Chen, Z., Dean-Ben, X. L., Gottschalk, S. & Razansky, D. Performance of optoacoustic and fluorescence imaging in detecting deep-seated fluorescent agents. *Biomed. Opt. Express* **9**, 2229–2239 (2018).
139. Laramie, M. D., Smith, M. K., Marmarchi, F., McNally, L. R. & Henary, M. Small molecule optoacoustic contrast agents: an unexplored avenue for enhancing in vivo imaging. *Molecules* **23**, 2766 (2018).
140. Tang, R. et al. A pilot study evaluating shaved cavity margins with micro-computed tomography: a novel method for predicting lumpectomy margin status intraoperatively. *Breast J.* **347**, 485–489 (2013).
141. McClatchy, D. M. III, Zuurbier, R. A., Wells, W. A., Paulsen, K. D. & Pogue, B. W. Micro-computed tomography enables rapid surgical margin assessment during breast conserving surgery (BCS): correlation of whole BCS micro-CT readings to final histopathology. *Breast Cancer Res. Treat.* **172**, 587–595 (2018).
142. Zhang, X. et al. Effects of hydrogen bond acceptor ability of solvents on molecular self-assembly of sulfadiazine solvates. *J. Pharm. Sci.* **107**, 2823–2828 (2018).
143. Qiu, S.-Q. et al. Micro-computed tomography (micro-CT) for intraoperative surgical margin assessment of breast cancer: a feasibility study in breast conserving surgery. *Eur. J. Surg. Oncol.* **44**, 1708–1713 (2018).
144. Heidkamp, J. et al. Ex vivo MRI evaluation of prostate cancer: localization and margin status prediction of prostate cancer in fresh radical prostatectomy specimens. *J. Magn. Reson. Imaging* **47**, 439–448 (2018).
145. Heidkamp, J. et al. MRI evaluation of vulvar squamous-cell carcinoma in fresh radical local excision specimens for cancer localization and prediction of surgical tumour-free margins. *NMR Biomed.* **32**, e4025 (2019).
146. Dashevsky, B. Z. et al. The potential of high resolution magnetic resonance microscopy in the pathologic analysis of resected breast and lymph tissue. *Sci. Rep.* **5**, 17435 (2015).
147. Steens, S. C. A. et al. Evaluation of tongue squamous cell carcinoma resection margins using ex-vivo MR. *Int. J. Comput. Assist Radiol. Surg.* **12**, 821–828 (2017).
148. van Oostenbrugge, T. J. et al. MRI as a tool to assess surgical margins and pseudocapsule features directly following partial nephrectomy for small renal masses. *Eur. Radiol.* **29**, 509–516 (2019).
149. Veeratterapillay, R. et al. Intraoperative and surgical specimen (ex vivo) ultrasound in the assessment of margins at partial nephrectomy. *Int. Urol. Nephrol.* **47**, 1665–1669 (2015).
150. Yamamoto, H. et al. Micrometastasis volume in lymph nodes determines disease recurrence rate of stage ii colorectal cancer: a prospective multicenter trial. *Clin. Cancer Res.* **22**, 3201–3208 (2016).
151. Ho, A. S. et al. Metastatic lymph node burden and survival in oral cavity cancer. *J. Clin. Oncol.* **35**, 3601–3609 (2017).
152. Toom, Den, I. J. et al. Sentinel node biopsy for early-stage oral cavity cancer: the VU University Medical Center experience. *Head Neck* **37**, 573–578 (2015).
153. Ferrer, R. Lymphadenopathy: differential diagnosis and evaluation. *Am. Fam. Physician* **58**, 1313–1320 (1998).
154. Liu, M., Wang, S. J., Yang, X. & Peng, H. Diagnostic efficacy of sentinel lymph node biopsy in early oral squamous cell carcinoma: a meta-analysis of 66 studies. *PLoS ONE* **12**, e0170322 (2017).
155. Donker, M. et al. Breast-conserving treatment with or without radiotherapy in ductal carcinoma in situ: 15-year recurrence rates and outcome after a recurrence, from the EORTC 10853 randomized phase III trial. *J. Clin. Oncol.* **31**, 4054–4059 (2013).
156. Marinovich, M. L. et al. The association of surgical margins and local recurrence in women with ductal carcinoma in situ treated with breast-conserving therapy: a meta-analysis. *Ann. Surg. Oncol.* **23**, 3811–3821 (2016).
157. Servoll, E. et al. The length of a positive surgical margin is of prognostic significance in patients with clinically localized prostate cancer treated with radical prostatectomy. *Urol. Int.* **93**, 289–295 (2014).
158. Hinni, M. L. et al. Surgical margins in head and neck cancer: a contemporary review. *Head Neck* **35**, 1362–1370 (2013).
159. Buchakjian, M. R., Tasche, K. K., Robinson, R. A., Pagedar, N. A. & Sperry, S. M. Association of main specimen and tumour bed margin status with local recurrence and survival in oral cancer surgery. *JAMA Otolaryngol. Head. Neck Surg.* **142**, 1191–1198 (2016).
160. *NCCN Guidelines: Treatment by Cancer Type* (National Comprehensive Cancer Network, 2019); https://www.nccn.org/guidelines/category_1
161. Gao, R. W. et al. Determination of tumour margins with surgical specimen mapping using near-Infrared fluorescence. *Cancer Res.* **78**, 5144–5154 (2018).
162. Wong, L. S. et al. Influence of close resection margins on local recurrence and disease-specific survival in oral and oropharyngeal carcinoma. *Br. J. Oral Maxillofac. Surg.* **50**, 102–108 (2012).
163. Gephardt, G. N. & Zarbo, R. J. Interinstitutional comparison of frozen section consultations. A college of American Pathologists Q-Probes study of 90,538 cases in 461 institutions. *Arch. Pathol. Lab. Med.* **120**, 804–809 (1996).
164. Mapstone, N. P. *Dataset for the Histopathological Reporting of Oesophageal Carcinoma (2nd edition)* (The Royal College of Pathologists, 2007).
165. Shi, C. *Protocol for the Examination of Specimens from Patients with Carcinoma of the Esophagus* (College of American Pathologists, 2017).
166. Kench, J. G. et al. Dataset for the reporting of prostate carcinoma in radical prostatectomy specimens: updated recommendations from the International Collaboration on Cancer Reporting. *Virchows Arch.* **475**, 263–277 (2019).
167. Faruqi, A. & Rous, B. *Standards and Datasets for Reporting Cancers. Dataset for Histopathological Reporting of Vulval Carcinomas* (The Royal College of Pathologists, 2018).
168. Slater, D. & Cook, M. *Standards and Datasets for Reporting Cancers. Dataset for Histopathological Reporting of Primary Cutaneous Malignant Melanoma and Regional Lymph Nodes* (The royal college of pathologists, 1–49 (2019).
169. Fisher, C. *Standards and Datasets for Reporting Cancers. Dataset for Histopathological Reporting of Soft Tissue Sarcomas* (The Royal College of Pathologists, 2018).
170. Wharton, S. B. et al. *Standards and Datasets for Reporting Cancers. Dataset for Tumours of the Central Nervous System, Including the Pituitary Gland* (The Royal College of Pathologists, 2016).
171. Nicholson, A. G., Kerr, K. & Grosney, J. *Standards and Datasets for Reporting Cancers. Dataset for Histopathological Reporting of Lung Cancer* (The Royal College of Ppathologists, 2018).
172. Campbell, F., Cairns, A., Duthie, F. & Freakins, R. *Dataset for the Histopathological Reporting of Carcinomas of the Pancreas, Ampulla of Vater and Common Bile Duct* (The Royal College of Pathologists, 2017).
173. Ellis, I. O. et al. *Pathology Reporting of Breast Disease in Surgical Excision Specimens Incorporating the Dataset for Histological Reporting of Breast Cancer* (The Royal College of Pathologists, 2016).
174. Loughrey, M. B., Quirke, P. & Shepherd, N. A. *Standards and Datasets for Reporting Cancers. Dataset for Histopathological Reporting of Colorectal Cancer* (The Royal College of Pathologists, 2018).
175. McCluggage, W. G. et al. Data set for the reporting of carcinomas of the cervix: recommendations from the International Collaboration on Cancer Reporting (ICCR). *Int. J. Gynecol. Pathol.* **37**, 205–228 (2018).
176. Jones, K. D. et al. Data set for reporting of lung carcinomas: recommendations from International Collaboration on Cancer Reporting. *Arch. Pathol. Lab. Med.* **137**, 1054–1062 (2013).

Acknowledgements

We thank G.W.'t Hooft (Philips Research) and M. Pleitez (Helmholtz Zentrum Munich) for useful discussions on nonlinear imaging techniques and Raman imaging, respectively. V.N. received funding from the EU grants SENSITIVE, funded by the European Union's Horizon 2020 research and innovation programme under grant agreement no. 801347, and ESCEND, funded by the Bundesministerium für Bildung und Forschung, Bonn, Germany (01KT1809) under the EU framework programme Horizon 2020 (TRANSCAN-2; grant agreement no. 643638).

Author contributions

F.J.V., J.V., M.J.H.W. and G.M.v.D. designed the study. F.J.V. and J.V. performed literature research and drafted the manuscript. P.J.v.d.Z. and V.N. provided technical input on imaging techniques. B.v.d.V. and S.K. provided input on clinical implementation. P.J.v.d.Z., M.J.H.W. and G.M.v.D. supervised the study and the writing of the manuscript. All authors contributed to revising the manuscript.

Competing interests

B.v.d.V. is a member of the Scientific Advisory Board of Visiopharm, for which compensation is received by the University Medical Center Groningen. V.N. is an equity owner and consultant of iThera Medical GmbH, an owner of Spear UG and a member of the Scientific Advisory Board of SurgVision B.V./Bracco Sp.A. P.J.v.d.Z. is an employee of Philips Research, The Netherlands. G.M.v.D. is CEO, founder and shareholder of TRACER Europe BV/AxelaRx. The other authors declare no competing interests.

Additional information

Correspondence should be addressed to Gooitzen M. van Dam.

Peer review information *Nature Biomedical Engineering* thanks the anonymous reviewer(s) for their contribution to the peer review of this work.